

## Keyhole depth instability in case of CW CO<sub>2</sub> laser beam welding of mild steel

N KUMAR\*, S DASH, A K TYAGI and BALDEV RAJ

Surface and Nanoscience Division, Indira Gandhi Centre for Atomic Research,  
Kalpakkam 603 102  
e-mail: niranjan@igcar.gov.in

MS received 5 August 2009; revised 27 November 2009; accepted 30 November 2009

**Abstract.** The study of keyhole (KH) instability in deep penetration laser beam welding (LBW) is essential to understand welding process and appearance of weld seam defects. The main cause of keyhole collapse is the instability in KH dynamics during the LBW process. This is mainly due to the surface tension forces associated with the KH collapse and the stabilizing action of vapour pressure. A deep penetration high power CW CO<sub>2</sub> laser was used to generate KH in mild steel (MS) in two different welding conditions i.e. ambient atmospheric welding (AAW) and under water welding (UWW). KH, formed in case of under water welding, was deeper and narrower than keyhole formed in ambient and atmospheric condition. The number and dimensions of irregular humps increased in case of ambient and under water condition due to larger and rapid keyhole collapse also studied. The thermocapillary convection is considered to explain KH instability, which in turn gives rise to irregular humps.

**Keywords.** Ambient and under water welding; keyhole collapse; weld depth instabilities; humps.

### 1. Introduction

The high-power CO<sub>2</sub> laser sources with Gaussian beam distribution are currently used for welding of thick stainless steels (Binda *et al* 2004). In the case of LBW, heat and fluid flow in the weld pool can significantly influence the temperature gradients, cooling rates and the solidification process and these are directly associated with the shape and size of KH (Kou 2002). Theoretical work, in this regard has been limited to stationary and free oscillations of a KH. Eigen frequencies of KH instability characterizes radial, axial and azimuthal oscillations (Heyn *et al* 1994; Dowden *et al* 1987; Kroos *et al* 1993a; Klein *et al* 1994; Kroos *et al* 1993b; Trappe *et al* 1994). So far, experimental data are available only for laser power fluctuations averaged over the beam cross section. In this regard, authors have limited themselves to study

\*For correspondence

only radial oscillations of KH (Klein *et al* 1996). It is shown that the cylindrical KH is held open and stabilized by a pressure balance combined with an energy balance (Kroos *et al* 1993a; Klein *et al* 1994; Kroos *et al* 1993b). The vapour recoil pressure tends to open the KH while surface tension acts to collapse it. The KH is surrounded by a pool of molten metal. The interface between the KH and melt pool is a free moving surface. The quasi-static behaviour of the KH stability is studied by pressure balance (Aalderink *et al* 2007). In case of elongated KH welds, a layer with solidified material forms at both sides of the KH. In combination with the melt pool behind the KH, this results in a bead shape with grooves along the bead edge (Beretta & Previtali 2009). In case of a circular KH, collapse of the rear KH wall is responsible for the strong surface waves on the melt pool. In case of the elongated KH, these collapses no longer occur. This brings out a strong reduction of melt pool surface waves and promotes smoother weld bead formation after solidification. The flow of the liquid-vapour generated by laser energy absorption inside the KH and the induced friction on the KH/melt pool wall are considered along with the surface tension. The buoyancy forces and forces exerted by surface tension are important mechanisms responsible for the melt pool movements linked with the KH instabilities (Amara & Fabbro 2008; Matsunawa *et al* 1998; Fabbro & Chouf 2000). It is inferred from various theoretical and experimental works that KH oscillation and collapses during LBW are linked to the KH instability (Heyn *et al* 1994; Dowden *et al* 1987; Kroos *et al* 1993a; Klein *et al* 1994; Kroos *et al* 1993b; Amara & Fabbro 2008; Matsunawa *et al* 1998; Fabbro & Chouf 2000). However, studies linking oscillations underneath KH with appearance of irregular humps in different media are rather sparse. Such studies can also be helpful in defining the effect of different media role involved in KH formation for enabling practical applications involving LBW.

In the present study, the KH instability and collapse are observed experimentally by carrying out CW CO<sub>2</sub> laser-induced KH formation on mild steel. The scale of instability at KH bottom has been investigated in both AAW and UWW conditions. The convection-diffusion equation has been analytically solved to explain thermocapillary motion that drives collapse of KH. This paper consists of the following sections. Section 2 briefly summarizes the experimental procedure of CW CO<sub>2</sub> laser keyhole formation in two different mediums. The obtained results are discussed in section 3 following the solution of convection–diffusion equation. This section also contains solution of the heat and mass transfer from the equation of viscous compressive melt flow in the ambient and underwater medium. Finally, section 4 concludes the study with some remarks on the achieved results and applications.

## 2. Experimental procedure

A high power CO<sub>2</sub> slab industrial laser, operated at a power of up to 3.5 kW in CW mode and linearly polarized with wavelength 10.64 μm, was used in the present experiments. The spatial mode was TEM<sub>00</sub> with a beam divergence of 0.5 mrad and the beam quality (M<sup>2</sup>) was 0.9. The focal distance was 300 mm and beam diameter at the specimen was 0.8 mm. The specimen was kept at the focal point of laser beam in each experiment. The schematic of experimental set-up is shown in figure 1. The beam is transported from reflected optical mirrors 2, 3 and transmitted through the collimator 4 to the specimen 6. Figure 1 shows a typical KH, 5 formed where  $r_{kh}$  and  $h_{kh}$  represent KH radius and depth, respectively,  $L_{wp}$  and  $M_{th}$  refer to the length of weld pool and material thickness,  $V_{wel}$  is the direction of specimen velocity. During this high power LBW process for MS specimen, localized heating caused evaporation of material. Sustained irradiation with power density exceeding 10<sup>6</sup> Wcm<sup>-2</sup> gave

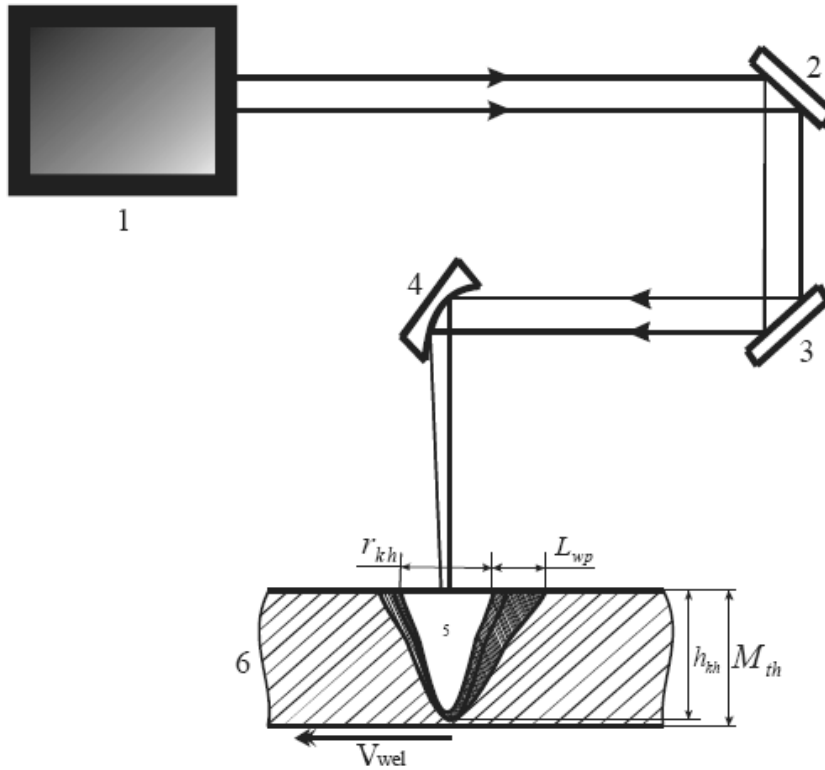


**Figure 1.** Schematic of CW CO<sub>2</sub> slab laser in the process of KH formation in welding mode, where 1 denotes CW CO<sub>2</sub> laser, 2, 3 are fully reflected mirrors, 4 is collimator, 5 is typical shape of KH, 6 is sample of MS.

rise to a deep penetration KH. Laser welding tests were performed on 7 mm thick plates of mild steel. The physical properties of mild steel such as density, specific heat, melting point and thermal conductivity were obtained from literature (Krauss 2005). In this experiment, KHs were obtained as a function of delivered laser power in AAW and UWW conditions. In UWW condition, the specimens were placed 1.5 mm deep inside the water. Specimens were fastened to an automated translation stage capable of achieving a constant speed of 2 m/min for both conditions. In this experiment, laser and welding parameters were kept similar for both cases to enable a comparative study pertaining to KH stability.

### 3. Results and discussion

The KH dimensions obtained at different laser powers in both the above conditions are shown in figure 2. The KH depth and width is found to increase linearly with laser power for both the conditions. The depth of KH ranges between 1.5 mm and 5.5 mm in the laser power range 0.5 kW to 3.5 kW. However, it is observed that KH is significantly less deep in case of AAW condition. In addition, KH is found to be slightly wider in case of AAW than KH formed in UWW condition. The width typically ranges between 0.6 and 1.6 mm at a depth equal to half of the maximum KH depth for a laser power range 0.5–3.5 kW for the both conditions,

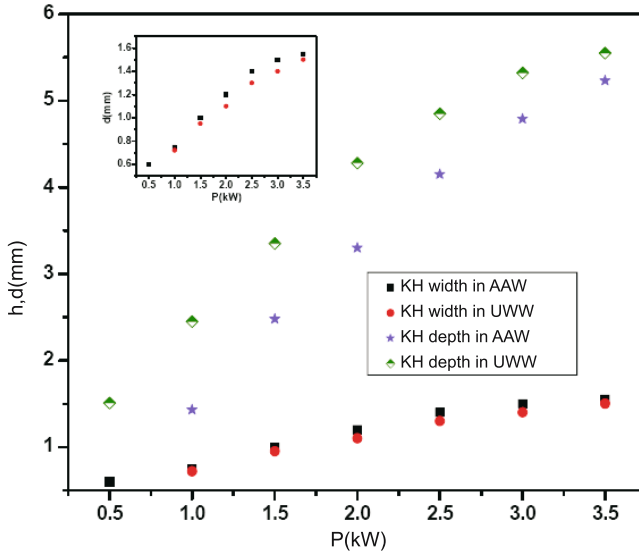


**Figure 2.** Keyhole dimension in both the AAW and UWW conditions as a function of incident laser power, in x-axis  $h$  and  $d$  denotes keyhole depth and width, respectively. In inset width of keyhole is drawn as a function of laser power.

as shown in the inset of figure 2. It has also been observed by Krauss (2005); Nakata & Oishi (1998) that weld width is smaller in case of UWW than that in AAW condition due to rapid cooling conditions. For laser power of 0.5 kW, there was no KH formation in AAW conditions whereas a 1.5 mm deep KH was formed in UWW condition. This can be explained on the basis of deeper penetration caused by excess hydrostatic pressure and vapour recoil pressure relative to surface tension force along the KH axis. This also indicates enhanced hydrodynamic stability of KH. The dimensions of KH are also found to stabilize at higher laser powers, as shown in figure 2. Typical optical micrographs of bottom of the KH formed at a laser power of 3.0 kW under AAW and UWW conditions are shown in figures 3 a and b, respectively. It is observed that depth of KH has comparatively less degree of oscillation in case of UWW than KH formed in AAW condition. The size of humps is also larger and more irregular at bottom of KH in case of AAW. This clearly exhibits rapid oscillations and eventual collapse of KH formed in AAW condition. The measured and analytically calculated values of oscillations at the bottom of the KH is presented in figure 4 along a typical weld length ( $L_{wp}$ ) of 2 mm. Both AAW and UWW depict periodic collapse of KH. Experimentally, the KH oscillation is absent for UWW conditions while it is significant in AAW conditions. UWW depict much lower magnitude of KH collapse. However, measured average peak maximum oscillation in both the conditions is found to be lower than the calculated analytical values. This can be attributed to various instability mechanisms present in real experimental conditions, as discussed above, only thermocapillary convection is considered for analytical calculations.

The temperature profile in KH has been calculated using convection diffusion equation (1) by considering necessary material parameters for CW  $\text{CO}_2$  laser. Figure 5 shows calculated temperature profile up to KH depth of 1 mm. Temperature is found to decrease along the KH depth. It is higher (1120 K) at the surface of the KH and lower (350 K) at the distance of 1 mm. The temperature  $\Delta T$  increases and oscillates at the front wall of KH. It oscillates between 1050 and 1400 K. It is also shown that the Marangoni number is higher than Reynolds number which indicates that capillary convection is higher than melt motion in the weld pool of KH. Both Marangoni and Reynolds numbers oscillate as a function of weld depth. The dominating factor of Marangoni number explains thermocapillary-induced convection.

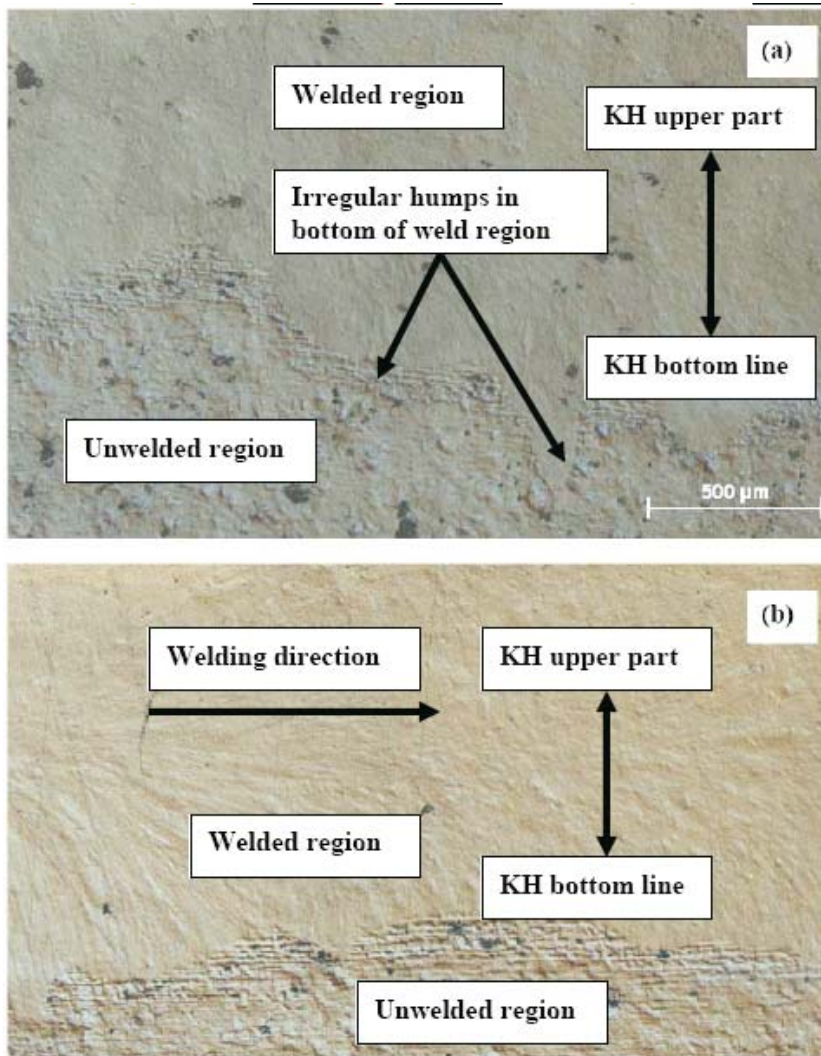


**Figure 3.** Typical optical micrographs of bottom of the keyhole; (a) AAW, (b) UWW condition.

The stability of KH depends on a balance between surface tension and vapour pressure which stabilizes KH geometry (Fabbro & Chouf 2000). Large scale turbulence and eddies are remarkably absent during the KH welding due to loss of rapid convection taking place in case of UWW condition (Mirzoev 1994). It is well understood that the Marangoni forces initiated by the surface tension gradients have considerable effect on the thermal transfer in the molten pool and this consequently leads to weld pool enlargement in the direction of capillary-oscillatory flow (Semak *et al* 1999; Golubev 1998). Liquid-vapour phase also appears in the KH region where various hydrodynamical phenomena such as, Marangoni convection, hydrostatic force, vapour recoil pressure and thermocapillary force operate. These phenomena creates KH instabilities such as Raleigh–Taylor, Kelvin–Helmholtz, capillary–oscillatory, thermocapillary and evaporation-recoil-driven melt expulsion (Mirzoev 1994;

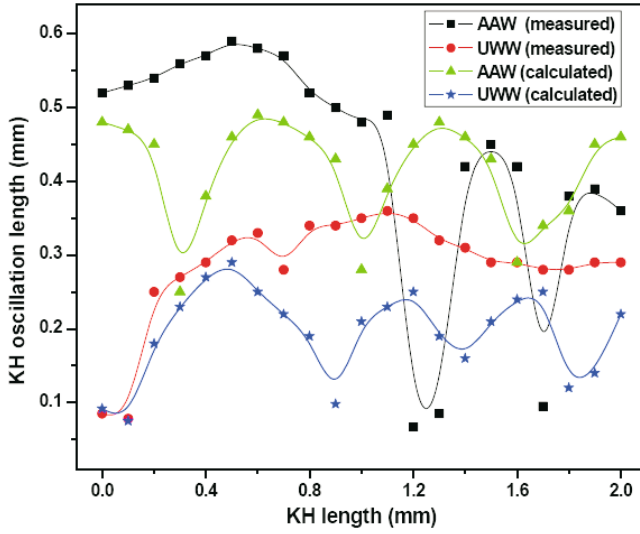


Figure 4. Keyhole oscillations versus weld pool length in both AAW and UWW conditions.

Semak *et al* 1999; Golubev 1998). If the temperature difference between the melt and solid phases is small, the induced flow becomes steady and axisymmetric (Rai *et al* 2008; Kamotani *et al* 2003; McNaught *et al* 1997). This temporal variation in flow patterns is motivated by surface tension fluctuations. Fluid flow pattern is also the primary cause for KH oscillation (Kumar *et al* 2007). A developed mould at the top of the fusion zone (FZ) is observed in UWW due to rapid melt solidification of molten material arising due to incidence of higher laser power. This causes restoring of melt movement and vapour pressure. The mould totally disappears and creates humps at the top of KH in the case of AAW condition due to excess vapour pressure. This hump at the mouth of KH is significant for higher laser power (Kumar *et al* 2010). This phenomena has also been observed in the bottom of KH in the present study.

The hardness of weld region rises up to 14.7 GPa in both the welding conditions. This is higher than the hardness of solid–liquid interface which ranges between 6 and 10 GPa in both

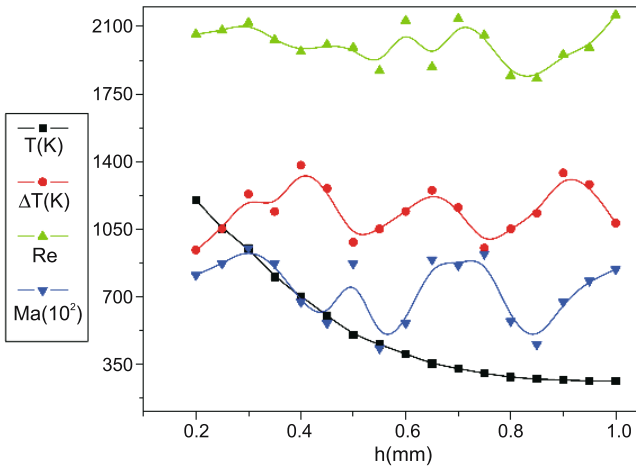


Figure 5. Thermal-induced Ma and Re number versus weld depth at 3.0 kW laser power.

the wedging condition (Kumar *et al* 2009). This reverts to the hardness of MS (3.4 GPa) away from KH on both sides. It shows that welding media does not affect on hardness of weld region.

The convection–diffusion equation has been applied to find out the thermal boundary at bottom of the KH to estimate KH oscillation. The governing form of convection–diffusion equation is written as:

$$\frac{\partial \rho u}{\partial t} + \frac{\partial \rho h V_m}{\partial x} = \nabla \cdot (\lambda \nabla T) + Q. \quad (1)$$

Here  $u$  is the internal energy,  $h$  is the enthalpy,  $\rho$  is the melt density,  $\lambda$  is the thermal conductivity,  $Q$  is volumetric heat source,  $T$  is temperature and  $V_m$  is the speed of either the heat source or the medium. In this particular application, the origin of the coordinate system is fixed to the centre of the heat source on top of the processed surface. The first term in equation (1) on the left hand side represents the change of internal energy and the second is a convective term. On the right hand side, there is the conductive term and a heat source or sink. For  $V_m = 0$ , this equation becomes the heat conduction equation. Here  $du = C_{f,s} dT$ , with  $C_{f,s}$  is the heat capacity of melt and solid phase. For the purpose of calculating heat and mass transfer from the equation of viscous compressive melt flow, velocity  $V$  and temperature  $T$  can be written as follows:

$$\text{div} V = 0, \quad (2)$$

$$\frac{\partial V}{\partial t} + (V \text{grad}) V = -\frac{1}{\rho_f} \text{grad} p + \nu \Delta V, \quad (3)$$

$$C_f \rho_f \frac{\partial T}{\partial t} + C_f \rho_f \text{div}(VT) - \text{div}(\lambda_f \text{grad} T) = 0. \quad (4)$$

Temperature distribution  $T$  in the solid phase can be written as follows:

$$C_s \rho_s \frac{\partial T}{\partial t} - \text{div}(\lambda_s \text{grad} T) = 0, \quad (5)$$

where  $p$  refers to the melt pressure,  $C_f$  and  $C_s$  are specific heat of liquid and solid phases, respectively,  $\lambda_f$  and  $\lambda_s$  are coefficients of thermal conductivity of liquid and solid phases, respectively,  $\rho_f$  and  $\rho_s$  are densities of liquid and solid phases, respectively,  $\nu$  is the coefficient of kinematic viscosity. The following boundary conditions were used in obtaining the solution:

$$\begin{cases} V_s|_{z=0} = 0, \mu \frac{\partial V_r}{\partial z}|_{z=0} = \gamma \frac{\partial T}{\partial r} \\ \lambda_{f,s} \frac{\partial T}{\partial z}|_{z=0} = \beta W(r, t). \end{cases} \quad (6)$$

Here  $\mu$  is coefficient of dynamic viscosity,  $\gamma$  is defined as  $\gamma = \frac{\partial \sigma}{\partial T}$ , where  $\sigma$  is surface tension,  $\beta(T)$  is coefficient of laser beam absorption on the surface of material,  $W(r, t)$  is distribution of laser power on the specimen surface. Once convection–diffusion term in equation (1) describes thermal boundary of KH oscillation, the Marangoni number can be applied for calculation of thermo-capillary-induced instability (Limmaneevichitr & Kou 2000). This is proportional to (thermal-) surface tension force relative to viscous force:

$$Mg = -\frac{\partial \sigma}{\partial T} \frac{1}{\mu \alpha} L_{kh} \Delta T. \quad (7)$$

Here  $L_{kh}$  is the characteristic length of KH,  $\alpha = \frac{\lambda}{\rho C_{s,f}}$  is thermal diffusivity,  $\mu$  represents dynamic viscosity at a given temperature,  $\lambda$  is the thermal conductivity,  $\Delta T$  is temperature difference between melt and melt-solid interface in the KH. The spatial gradient of surface tension yields Marangoni stress. Solving these equations (1–5) with boundary conditions (6) defines oscillation of thermal boundary in the bottom of KH where convection–diffusion and thermocapillary mechanisms are taken in to account to calculate thermal instabilities which is accountable for KH depth oscillation. The melt flow characteristics can be defined as Reynolds–Marangoni number expressed as  $Re = \frac{\gamma \Delta T H^2}{\mu \nu R}$ , where  $\frac{\Delta T}{R}$  is characteristic temperature gradient of the melt surface,  $H$  and  $R$  are melt depth and radius, respectively.

#### 4. Conclusions

Laser beam welding of MS has been carried out in the AAW and UWW conditions using CW CO<sub>2</sub> slab laser to study dynamics of KH instability. In both conditions, KH dimensions are found to increase as a function of laser power. Laser power causing rise in KH depth is found to be higher in case of UWW as compared to AAW. Analytical results show periodic KH collapse in both the welding conditions. A good agreement between measured and analytically calculated KH oscillation length has been found. In analytical calculations, only thermocapillary-induced instability is considered whereas in actual experimental practice, several other phenomena including mechanically-induced instabilities manifest. The magnitude of KH collapse is found to be higher in case of AAW condition due to capillary convective induced oscillation. In case of KH formed in UWW condition, the frequency of KH collapse is relatively low. It can be concluded that the medium is one of the primary element for thermocapillary-induced instability of KH. The present study also invoked the significance of laser parameters used in LBW carried out in different media.

The authors would like to thank Prof. A V Fedin and Dr. A A Govrilov from Kovrov State Technological Academy, Russia and V S Golubev from Institute on Laser and Information Technologies, Russian Academy of Sciences (RAS), Russia for invaluable discussions. Authors also thank the team of Centre for Laser Processing, International Advanced Research Centre for Powder Metallurgy and New Materials (ARCI) for providing experimental facilities. Dr. N Kumar specially thanks Mr. S Kataria for invaluable discussions.

#### List of symbols

$r_{kh}$ and $h_{kh}$	keyhole radius and depth, respectively (mm)
$L_{wp}$	length of weld pool (mm)
$M_{th}$	material thickness (mm)
$L_{kh}$	characteristic length of KH (mm)
$u$	internal energy (J kg <sup>-1</sup> )
$h$	enthalpy (J kg <sup>-1</sup> )
$\rho$	mass density of the melt (kg m <sup>-3</sup> )
$\chi$	coefficient of thermal conductivity (W m <sup>-1</sup> K <sup>-1</sup> )
$Q$	volumetric heat source
$V$	melt flow velocity (m/s)

$T$	temperature (K)
$V_m$	speed of either the heat source or the medium (m/min)
$p$	melt pressure (Pa)
$C_f$ and $C_s$	specific heat of liquid and solid phases, respectively (J kg <sup>-1</sup> K <sup>-1</sup> )
$\lambda_f$ and $\lambda_s$	coefficient of thermal conductivity of liquid and solid phases, respectively (W m <sup>-1</sup> K <sup>-1</sup> )
$\rho_f$ and $\rho_s$	density of liquid and melt phase, respectively (kg m <sup>-3</sup> )
$\nu$	kinematic viscosity (m <sup>2</sup> s <sup>-1</sup> )
$\mu$	dynamic viscosity (N s/m <sup>2</sup> )
$\sigma$	surface tension coefficient (N m <sup>-1</sup> )
$\beta(T)$	coefficient of laser beam absorption on the surface of material (W)
$W(r, t)$	distribution of laser power (W m <sup>-2</sup> )
$L_{kh}$	characteristic length of keyhole (mm)
$\alpha = \frac{\lambda}{\rho C_{s,f}}$	thermal diffusivity (m <sup>2</sup> s <sup>-1</sup> )
$\lambda$	thermal conductivity (W m <sup>-1</sup> K <sup>-1</sup> )
$\Delta T$	keyhole front wall temperature at surface (K)
$H$ and $R$	melt depth and radius, respectively (mm)

## References

- Aalderink B J, Lange de D F, Aarts R G K M, Meijer J 2007 Keyhole shapes during laser welding of thin metal sheets. *J. Phys. D: Appl. Phys.* 40: 5388–5393
- Amara E H, Fabbro R 2008 Modelling of gas jet effect on the melt pool movements during deep penetration laser welding. *J. Phys. D: Appl. Phys.* 41: 055503–055513
- Beretta S, Previtali B 2009 Estimate of maximum pore size in keyhole laser welding of carbon steel. *Sci. Technol. Weld. Join.* 14: 106–116
- Binda B, Capello E, Previtali B 2004 A semi-empirical model of the temperature field in the AISI 304 laser welding. *J. Mater. Proc. Technol.* 155–156: 1235–1241
- Dowden J, Postacioglu N, Davis M, Kapadia P 1987 A keyhole model in penetration welding with a laser. *J. Phys. D: Appl. Phys.* 20: 36–44
- Fabbro R, Chouf K 2000 Dynamical description of the keyhole in deep penetration laser welding. *J. Laser Appl.* 12: 142–148
- Golubev V S 1998 Nonstationary hydrodynamics in processes of laser beam-material interaction. *Proc. SPIE* 3688: 108–118
- Heyn H, Decker I, Wohlfahrt H 1994 Tools and requirements for in-process quality control in laser beam welding. *Proc. SPIE* 2207: 381–91
- Kamotani Y, Wang L, Hatta S, Wang A, Yoda S 2003 Free surface heat loss effect on oscillatory thermocapillary flow in liquid bridges of high Prandtl number fluids. *Inter. J. Heat Mass Trans.* 46: 3211–3220
- Klein T, Vicanek M, Kroos J, Decker I, Simon G 1994 Oscillations of the keyhole in penetration laser beam welding. *J. Phys. D: Appl. Phys.* 27: 2023–2030
- Klein T, Vicanek M, Simon G 1996 Forced oscillations of the keyhole in penetration laser beam welding. *J. Phys. D: Appl. Phys.* 29: 322–332
- Kou S 2002 *Welding metallurgy*, Second edition (New York: John Wiley & Sons, Inc.)
- Krauss G 2005 *Processing, structure, and performance*. ASM Inter: Materials Park, Ohio, USA, OH 44073–0002
- Kroos J, Gratzke U, Simon G 1993a Towards a self-consistent model of the keyhole in penetration laser beam welding. *J. Phys. D: Appl. Phys.* 26: 474–80
- Kroos J, Gratzke U, Vicanek M, Simon G 1993b Dynamic behaviour of the keyhole in laser welding. *J. Phys. D: Appl. Phys.* 26: 481–486

- Kumar N, Dash S, Tyagi A K, Baldev Raj 2007 Hydrodynamical phenomena in the process of laser welding and cutting. *Sci. Technol. Weld. Join.* 12: 540–548
- Kumar N, Kataria S, Sanmugarajan B, Dash S, Tyagi A K, Padmnabham G, Baldev Raj 2010 Contact mechanical studies on CW CO<sub>2</sub> laser beam weld of mild steel with ambient and under water medium. *Materials and Design* 31: 3610–3617
- Limmaneevichitr C, Kou S 2000 Experiments to simulate effect of Marangoni convection on weld pool shape. *Weld. J.* 5: 126–135
- Matsunawa A, Kim J D, Seto N, Mizutani M, Katayama S 1998 Dynamics of keyhole and molten pool in laser welding. *J. Laser Appl.* 1: 247–254
- McNaught W, Deans W F, Watson J 1997 High power laser welding in hyperbaric and water environments. *J. Laser Appl.* 9: 129–136
- Mirzoev F K 1994 Evaporation-capillary instability in a deep vapour–gas cavity. *Kvant. Elektr.* 24: 138–140
- Nakata K, Oishi M 1998 Nuclear Power Systems. *Proc. Int. Conf. Env. Deg. Mat.*
- Rai R, Kelly S M, R. Martukanitz P, DevRoy T 2008 A convective heat-transfer model for partial and full penetration keyhole mode laser welding of a structural steel. *Metall. Mater. Trans. A* 39A: 98–112
- Semak V V, Bragg W D, Damkroger B, Kempka S 1999 Transient model for the keyhole during laser welding. *J. Phys. D: Appl. Phys.* 32: 61–64
- Trappe J, Tix C, Kroos J, Simon G 1994 On the shape and location of the keyhole in penetration laser welding. *J. Phys. D: Appl. Phys.* 27: 2152–2154